IOP PUBLISHING JOURNAL OF PHYSICS: CONDENSED MATTER
J. Phys.: Condens. Matter **24** (2012) 205503 (9pp) doi:10.1088/0953-8984/24/20/205503

Electronic structure of transparent oxides with the Tran–Blaha modified Becke–Johnson potential

H Dixit[1], R Saniz[1], S Cottenier[2], D Lamoen[3] and B Partoens[1]

[1] Departement Fysica, Universiteit Antwerpen, Groenenborgerlaan 171, BE-2020 Antwerpen, Belgium
[2] Center for Molecular Modeling, Ghent University, Technologiepark 903, BE-9052 Zwijnaarde, Belgium
[3] EMAT, Departement Fysica, Universiteit Antwerpen, Groenenborgerlaan 171, BE-2020 Antwerpen, Belgium

E-mail: Hemant.Dixit@ua.ac.be, Rolando.Saniz@ua.ac.be, Stefaan.Cottenier@UGent.be, Dirk.Lamoen@ua.ac.be and Bart.Partoens@ua.ac.be

Received 5 January 2012, in final form 30 March 2012
Published 27 April 2012
Online at stacks.iop.org/JPhysCM/24/205503

Abstract
We present electronic band structures of transparent oxides calculated using the Tran–Blaha modified Becke–Johnson (TB-mBJ) potential. We studied the basic n-type conducting binary oxides In_2O_3, ZnO, CdO and SnO_2 along with the p-type conducting ternary oxides delafossite $CuXO_2$ (X = Al, Ga, In) and spinel ZnX_2O_4 (X = Co, Rh, Ir). The results are presented for calculated band gaps and effective electron masses. We discuss the improvements in the band gap determination using TB-mBJ compared to the standard generalized gradient approximation (GGA) in density functional theory (DFT) and also compare the electronic band structure with available results from the quasiparticle GW method. It is shown that the calculated band gaps compare well with the experimental and GW results, although the electron effective mass is generally overestimated.

(Some figures may appear in colour only in the online journal)

1. Introduction

The binary oxides—In_2O_3, ZnO, CdO and SnO_2—form the basic set of host materials which are used as transparent conducting oxides (TCOs). Their wide band gap and highly dispersed conduction band make them a suitable choice for this purpose. Impurity-doped In_2O_3, ZnO, CdO and SnO_2, as well as ternary compounds such as $SnZn_2O_4$, $CdIn_2O_4$, $SnCd_2O_4$, $ZnSnO_3$, $Zn_2In_2O_5$, $Zn_3In_2O_6$, In_2SnO_4, $CdSnO_3$, and multi-component oxides consisting of combinations of these are the preferred materials for most present day applications [1, 2]. Most of these TCOs show n-type conductivity while a p-type conducting TCO is a relatively rare phenomenon. A well-known example of p-type TCO is the delafossite family $CuXO_2$ (X = Al, Ga, In) [3–7], while ZnX_2O_4 (X = Co, Rh, Ir) in the spinel structure has been recently studied as well [7–9]. The expanding use of TCO materials, especially for the production of transparent electrodes for optoelectronic device applications, demands ever better TCO materials [10, 11]. The key physical properties of an n-type TCO material are the band gap for optical transparency and the effective mass of the electron which determines the mobility of charge carriers. The application of electronic structure methods, capable of accurately calculating these quantities, is thus helpful in order to find new or better TCO materials.

The electronic structure of these metal–oxide semiconductors has been a subject of enduring interest. One important feature is the hybridization between the metal d orbitals and the oxygen p orbitals. Density functional theory (DFT) calculations can assess the strength of this hybridization. It is well known that the calculated Kohn–Sham (KS) [12, 13] band gaps obtained using popular approximations such as the local density approximation (LDA) or the generalized

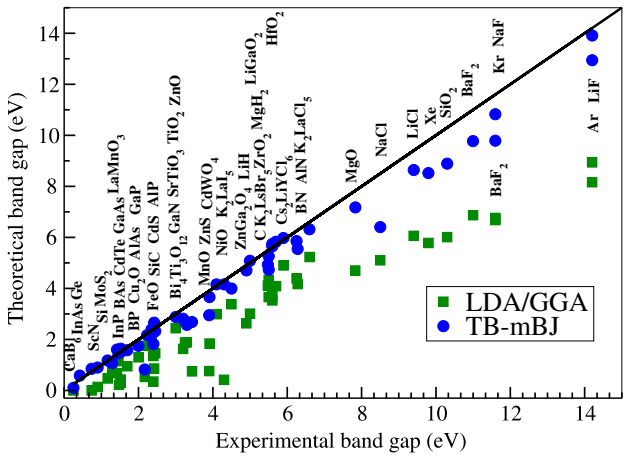

Figure 1. LDA/GGA and TB-mBJ versus experimental band gaps obtained from [21–31].

gradient approximation (GGA) are strongly underestimated. However, in principle, one cannot compare the KS gap with the experimental band gap since it differs from the experimental gap by the neglected derivative discontinuity Δ_{xc} [14, 15]. This Δ_{xc} is significant in the case of semiconductors and insulators and needs to be corrected. There are different schemes available, such as the optimized effective potential (OEP) [16, 17] method, hybrid functionals as proposed by Heyd, Scuseria, and Ernzerhof (HSE) [18, 19], etc, to improve the KS band gap. Unfortunately, these schemes are computationally expensive compared to the LDA or GGA. Also the GW approximation [20] to many-body perturbation theory, which represents the state of the art technique to calculate the quasiparticle correction to the band gap of solids, is computationally very demanding. However, the recently proposed Tran–Blaha modified version of the Becke–Johnson potential (TB-mBJ) [21] has proved to be a successful method for accurate band gaps of semiconductors and insulators, and computationally it is as economical as the LDA or GGA although its self-consistency cycle converges slower and therefore requires more iterations (a factor of 2–3). The TB-mBJ scheme is rapidly gaining popularity and a significant number of studies reporting the improvements in the band gaps have been published [21–31] since the original publication in 2009. An overview of all results available in the literature at present is given in figure 1. It is obvious from this data set that TB-mBJ predicts reasonable band gaps up to about 6 eV. In a few cases there are minor overestimations. Most of the deviations are small underestimations. For band gaps larger than 6 eV, the available data set suggests a tendency towards a small yet significant systematic underestimation. Occasionally there are cases where the deviation is rather large (Cu_2O, NaCl). Overall, TB-mBJ is a decent alternative for GW or hybrid functionals, achieving a comparable accuracy at a far lower cost.

In this paper, we apply TB-mBJ to a group of oxides that are either used for their optical properties, or have the potential to be so. The band gaps, band structures and effective electron masses obtained in this way are compared with what is predicted by the common Perdew–Burke–Ernzerhof (PBE) functional [32], and—where available—by G_0W_0. Trends in differences will be discussed.

2. Theory

The electronic structure of a periodic solid can be calculated using the well-known KS equations given by

$$(-\tfrac{1}{2}\nabla^2 + v_{\mathrm{eff},\sigma}^{\mathrm{K-S}}(\mathbf{r}))\psi_{i,\sigma}(\mathbf{r}) = \epsilon_{i,\sigma}\psi_{i,\sigma}(\mathbf{r}) \tag{1}$$

where $\psi_{i,\sigma}$ are the one-electron wave functions. The KS effective potential, $V_{\mathrm{eff},\sigma}^{\mathrm{KS}} = V_{\mathrm{ext}} + V_H + V_{\mathrm{xc},\sigma}$, is the sum of external, Hartree and exchange–correlation (xc) terms. In this, the last term needs to be approximated while the other two terms are calculated accurately. The popular approximations for the exchange–correlation energy are the LDA and GGA. Although the KS DFT is a fast and reliable method to calculate the electronic structure, the excited state properties like the band gap are severely underestimated for many semiconductors and insulators. Recently, Tran and Blaha have proposed an alternative scheme to improve the band gap calculation within DFT by modifying the Becke–Johnson potential which reads as follows:

$$v_{x,\sigma}^{\mathrm{BJ}}(\mathbf{r}) = v_{x,\sigma}^{\mathrm{BR}}(\mathbf{r}) + \frac{1}{\pi}\sqrt{\frac{5}{6}}\sqrt{\frac{t_\sigma(\mathbf{r})}{\rho_\sigma(\mathbf{r})}}. \tag{2}$$

Here, $\rho_\sigma = \sum_{i=1}^{N_\sigma}|\psi_{i,\sigma}|^2$ is the electron density, $t_\sigma = (1/2)\sum_{i=1}^{N_\sigma}\nabla^*\psi_{i,\sigma}\nabla^*\psi_{i,\sigma}$ is the kinetic-energy density and

$$v_{x,\sigma}^{\mathrm{BR}}(\mathbf{r}) = -\frac{1}{b_\sigma(\mathbf{r})}(1 - \mathrm{e}^{-x_\sigma(\mathbf{r})} - \tfrac{1}{2}x_\sigma(\mathbf{r})\mathrm{e}^{-x_\sigma(\mathbf{r})}) \tag{3}$$

is the Becke–Roussel (BR) exchange potential, which was proposed to model the Coulomb potential created by the exchange hole. In equation (3) , x_σ is determined from a nonlinear equation involving ρ_σ, $\nabla\rho_\sigma$, $\nabla^2\rho_\sigma$ and t_σ. The b_σ is calculated with $b_\sigma = [x_\sigma^3\mathrm{e}^{-x_\sigma}/(8\pi\rho_\sigma)]^{1/3}$.

Tran and Blaha have introduced a parameter 'c' to change the relative weights of the two terms in the BJ potential and the modified potential (TB-mBJ) reads

$$v_{x,\sigma}^{\text{TB-mBJ}}(\mathbf{r}) = cv_{x,\sigma}^{\mathrm{BR}}(\mathbf{r}) + (3c-2)\frac{1}{\pi}\sqrt{\frac{5}{6}}\sqrt{\frac{t_\sigma(\mathbf{r})}{\rho_\sigma(\mathbf{r})}}. \tag{4}$$

In [21] a prescription for calculating c is given by

$$c = \alpha + \beta\left(\frac{1}{V_{\mathrm{cell}}}\int_{\mathrm{cell}}\frac{|\nabla\rho(\mathbf{r}')|}{\rho(\mathbf{r}')}\,\mathrm{d}^3r'\right) \tag{5}$$

where V_{cell} is the unit cell volume and α and β are two free parameters whose values are $\alpha = -0.012$ and $\beta = 1.023$ Bohr$^{1/2}$ according to a fit to experimental results. The merits and limitations of this prescription are discussed in [31]. In the present work we further explore the performance of this scheme by applying it to TCOs with the c parameter determined from equation (5) .

3. Computational details

All-electron calculations with the APW + lo method were performed using the WIEN2k code [51, 52]. In this method,

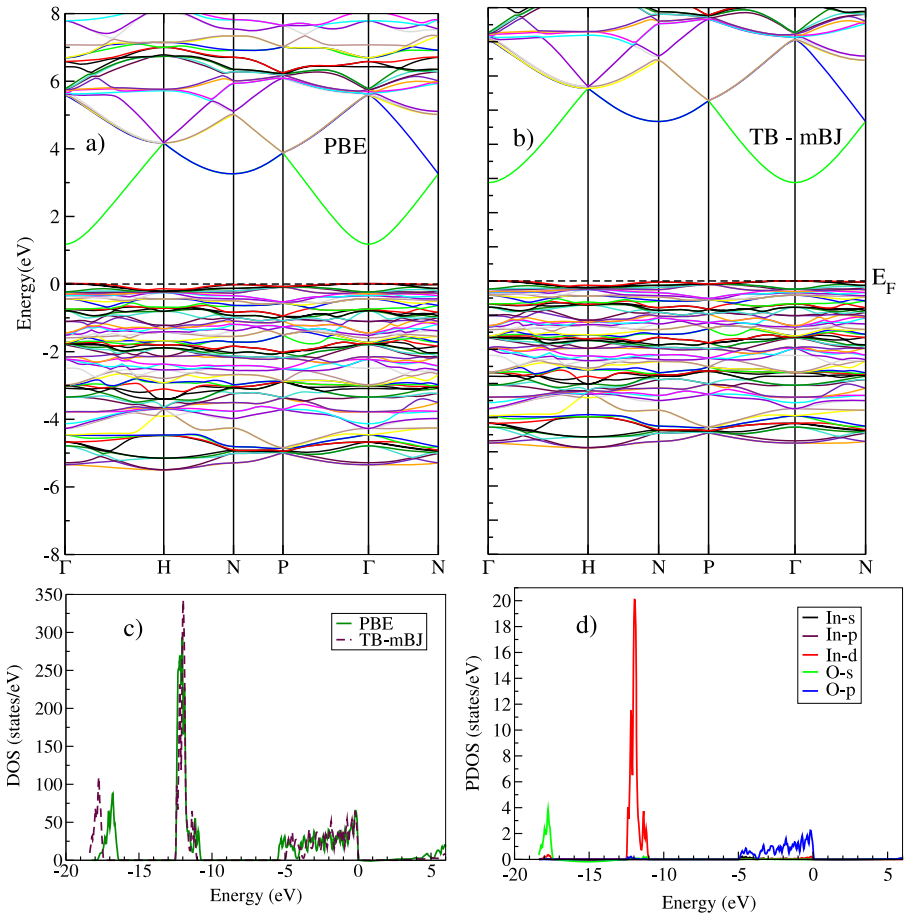

Figure 2. (a) PBE band structure, (b) TB-mBJ band structure, (c) total DOS with PBE, TB-mBJ, (d) PDOS with TB-mBJ for In_2O_3.

the wave functions are expanded in spherical harmonics inside non-overlapping atomic spheres of radius R_{MT} and in plane waves in the remaining space of the unit cell (the interstitial region). The radii for the muffin tin spheres were taken as large as possible without overlap between the spheres: $R_{MT}^{In} = R_{MT}^{Sn} = R_{MT}^{Ga} = R_{MT}^{Cu} = R_{MT}^{Rh} = R_{MT}^{Ir} = 2.1, R_{MT}^{Zn} = R_{MT}^{Cd} = R_{MT}^{Co} = 1.9, R_{MT}^{Al} = 1.6$, and $R_{MT}^{O} = 1.5$ bohr. The charge density was Fourier expanded up to $G_{max} = 12$ au^{-1}. The plane wave expansion of the wave function in the interstitial region was truncated at $R_{MT}K_{max} = 9$. A regular $4 \times 4 \times 4$ Monkhorst–Pack [38] k-point mesh was used for cubic structures such as In_2O_3, CdO, ZnX_2O_4 and also for the rhombohedral unit cell ($CuXO_2$). For the hexagonal unit cell a $3 \times 3 \times 2$ Monkhorst–Pack k-point mesh was used. All calculations were performed at the experimental lattice parameters, for a meaningful comparison.

4. Results

4.1. n-type binary oxides

4.1.1. Indium oxide. In_2O_3 has a body centered cubic bixbyite structure, with eight formula units per primitive cell. Each In atom is coordinated by six oxygen atoms in a distorted octahedron. The unit cell contains 40 atoms and the lattice constant is 10.12 Å.

The band structures along high symmetry lines in the Brillouin zone calculated with PBE and TB-mBJ are presented in figure 2. This figure shows that In_2O_3 is a direct band gap semiconductor. Although the widely quoted direct band gap of In_2O_3 is 3.75 eV and the indirect gap is 2.62 eV, recent experimental reinvestigation along with theoretical studies have concluded In_2O_3 to be a direct band gap semiconductor with a band gap of ∼3.1 eV [39]. The PBE band gap is 1.18 eV and is consistent with earlier reported results [40]. The TB-mBJ band structure shows a significant opening of the band gap and the calculated TB-mBJ gap is 2.90 eV, which compares well with both experiment and the G_0W_0 result of 3.1 eV.

We further analyze the band structure with the help of the density of states (DOS) and projected density of states (PDOS) plots as shown in the same figure. The PDOS shows that the valence band maximum (VBM) shows strong O p character and also an In d contribution indicative of p–d hybridization in In_2O_3. The low lying energy bands around −12 eV have a strong In d character while the lowest energy band around −18 eV has O s character. A comparison with the DOS obtained by PBE shows that the valence band dispersion in the TB-mBJ band structure has been narrowed by about 1 eV in the region 0 to −6 eV. The In d levels have similar positions while the O s band has moved to a higher binding energy of −19 eV with TB-mBJ.

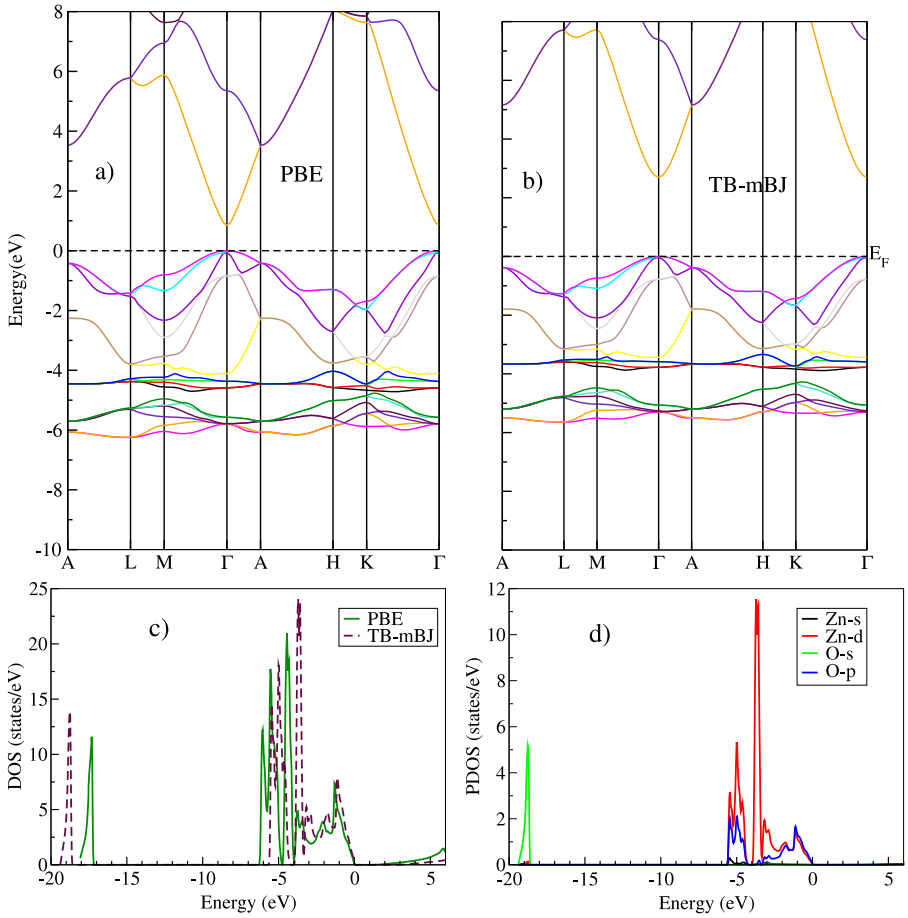

Figure 3. (a) PBE band structure, (b) TB-mBJ band structure, (c) total DOS with PBE, TB-mBJ, (d) PDOS with TB-mBJ for ZnO.

4.1.2. Zinc oxide. ZnO is a wide band gap semiconductor with a direct gap of 3.44 eV. ZnO crystallizes in the wurtzite structure with lattice parameters $a = 3.2489$ Å, $c = 5.2049$ Å, and internal parameter $u = 0.381$. The PBE band gap is 0.80 eV which opens up to 2.68 eV in the TB-mBJ band structure. The TB-mBJ gap is underestimated by 22% in comparison with experiment; however, it matches with the G_0W_0 result of 2.49–2.51 eV [43, 42]. The band structure and DOS are shown in figure 3. The lowest valence band plotted in the TB-mBJ band structure is around −5.4 eV which is ∼0.8 eV higher than the corresponding band in the PBE band structure. It is also clear from the total DOS plot that the valence band dispersion in TB-mBJ is narrowed compared to PBE. This narrowing is suggested to be the origin of the remaining discrepancy between the TB-mBJ and experimental band gaps by Singh [44]. The O s state which forms the lowest valence band is, however, at a higher binding energy in the TB-mBJ band structure compared with its PBE counterpart. The PDOS calculated with TB-mBJ shows a strong p–d hybridization between the Zn d and O p states in the region 0 to −6 eV. The Zn 3d states are placed around −5 eV and are shallow compared to the experimental estimate of ∼7–8 eV below the VBM.

4.1.3. Cadmium oxide. CdO has the rocksalt structure and is distinctly different from other IIB–VI binary oxides which are either cubic zinc-blende or hexagonal wurtzite structures. The metal cation is octahedrally coordinated in the rocksalt structure whereas in zinc-blende or wurtzite structure it is tetrahedrally coordinated. The octahedral point group (O_h) of the rocksalt structure contains an inversion center at the Γ point. As a consequence, the 'p' and 'd' states belong to a different representation at the Γ point in the rocksalt structure and do not mix. However, at other points with lower symmetry, the 'p' and 'd' states can mix in the Brillouin zone. Thus, in the case of CdO, the hybridization of O 2p derived orbitals with the Cd 4d states combined with the octahedral point symmetry leads to an indirect band gap.

The PBE band structure (see figure 4(a)) shows CdO to be semi-metallic since the conduction band minimum (CBM) crosses the Fermi energy level (E_f). We obtain an indirect band gap of 1.82 eV with TB-mBJ. Although the band gap is widely quoted to be 0.55 eV at room temperature and 0.84 eV at 100 K, McGuinness *et al* [45] have suggested a value of ∼1.2 eV, while their own x-ray emission and absorption measurements on high purity samples yield a value of almost 2 eV. Also, a recent G_0W_0 calculation results in a much larger value of 1.07 eV for the indirect gap [46]. Thus the calculated TB-mBJ gap is in agreement with the reported experimental range of 1.2–2 eV.

The DOS and PDOS plots for CdO (see figures 4(c), (d)) show a strong p–d hybridization, narrowing the valence band

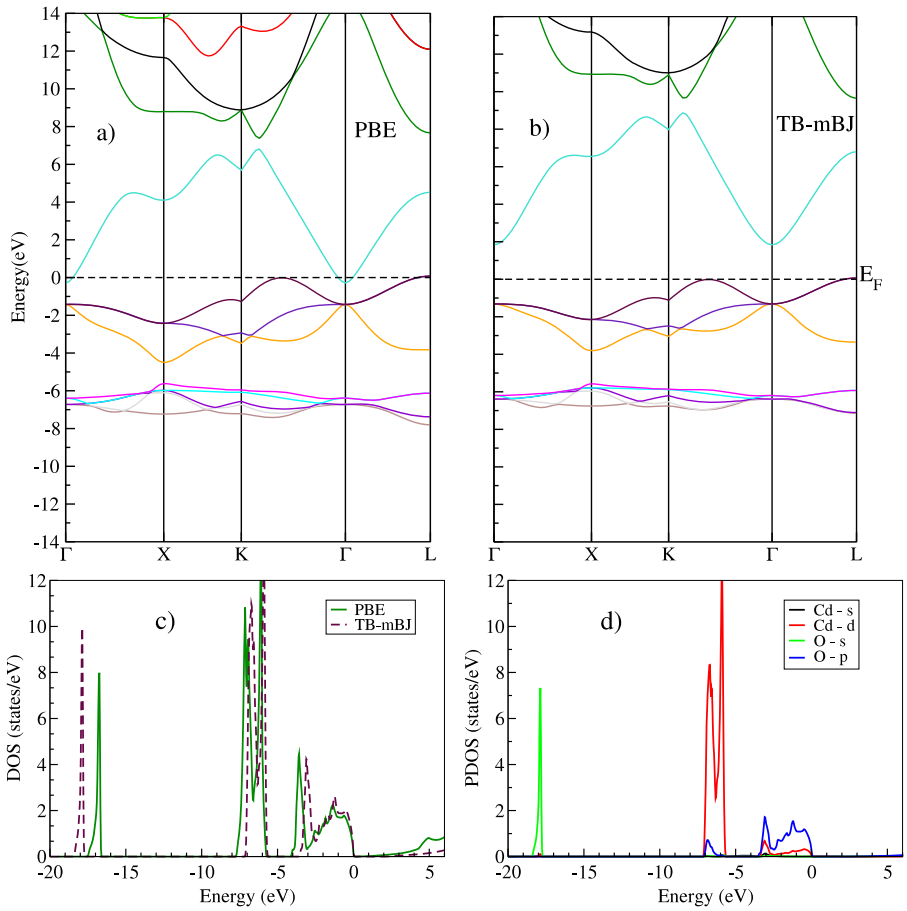

Figure 4. (a) PBE band structure, (b) TB-mBJ band structure, (c) total DOS with PBE, TB-mBJ, (d) PDOS with TB-mBJ for CdO.

similarly to ZnO. The Cd d energy levels around −6.5 eV are at higher binding energy compared to the experimental result of −8.8 eV below the VBM.

4.1.4. Tin dioxide. SnO_2 exists in rutile structure. The lattice parameters are $a = 4.7374$ Å, $c = 3.1864$ Å, and the internal parameter $u = 0.305$. The band structure shown in figure 5 yields a direct band gap of 1.25 eV for PBE and 3.20 eV for TB-mBJ. The reported experimental gap of SnO_2 is 3.60 eV [47]. Thus the TB-mBJ band gap shows ∼10% underestimation compared to experiment, but is still much improved compared to the PBE functional. The valence bands in the range of 0 to −7 eV are composed of O p and Sn s, p orbitals as evident from the PDOS presented in figure 5. There is also hybridization between the Sn d and O s orbitals for the lowest valence bands between −16 and −19 eV. These Sn d orbitals are at lower binding energy in comparison with the reported experimental value of 21.1–21.4 eV [48]. Unlike the other oxides, a distinct p–d hybridization is not observed in the PDOS.

The TB-mBJ total DOS shows that the valence band dispersion is reduced compared to the PBE band structure. This suggests that the TB-mBJ scheme tends to localize the valence bands compared to their PBE counterparts. This feature is found to be common for all the oxides studied and is more pronounced for widely dispersed bands than localized states such as O s.

4.2. p-type ternary oxides

We now present the TB-mBJ electronic structures of p-type ternary oxides: the delafossite $CuXO_2$ (X = Al, Ga, In) family and ZnX_2O_4 (X = Co, Rh, Ir) in the spinel structure. The delafossite crystal structure (space group $R\bar{3}m$, #166) is composed of O–Cu–O dumbbell layers in a hexagonal plane separated by an XO_6 edge-sharing octahedral layer. The spinel (space group $Fd\bar{3}m$, #227) lattice is based on face centered cubic packing of oxygen atoms (32 e sites) which are tetrahedrally coordinated with Zn ions (eight a sites) and octahedrally coordinated with the X cations (16 d sites). The experimental lattice constants are listed in table 3.

The TB-mBJ calculated band structures and PDOSs of the delafossite family are shown in figure 6. All three compounds have an indirect fundamental band gap with the CBM at Γ and the VBM near F along the Γ–F direction. As seen in the PDOS, the well-isolated peak in the region 2–4 eV is the CBM which is composed of Cu d and O p orbitals. In the valence band the Cu d states are placed close to the Fermi level with a pronounced peak around −1.8 eV. These states are shallow compared to the XPS measurements of about −2.8 eV by Aston *et al* [53]. The calculated indirect band gaps are 2.21, 1.35 and 0.82 eV for $CuAlO_2$, $CuGaO_2$ and $CuInO_2$ respectively. We also list in table 4 the direct gaps at the L point since the optically allowed transition is

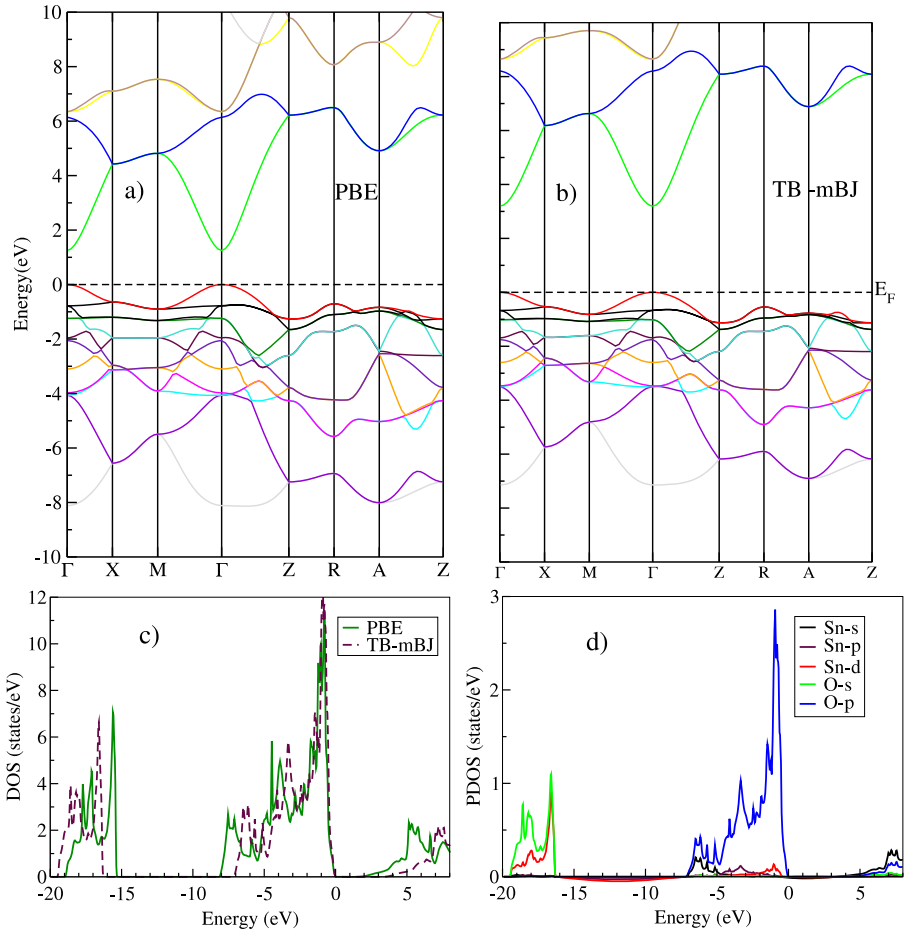

Figure 5. (a) PBE band structure, (b) TB-mBJ band structure, (c) total DOS with PBE, TB-mBJ, (d) PDOS with TB-mBJ for SnO_2.

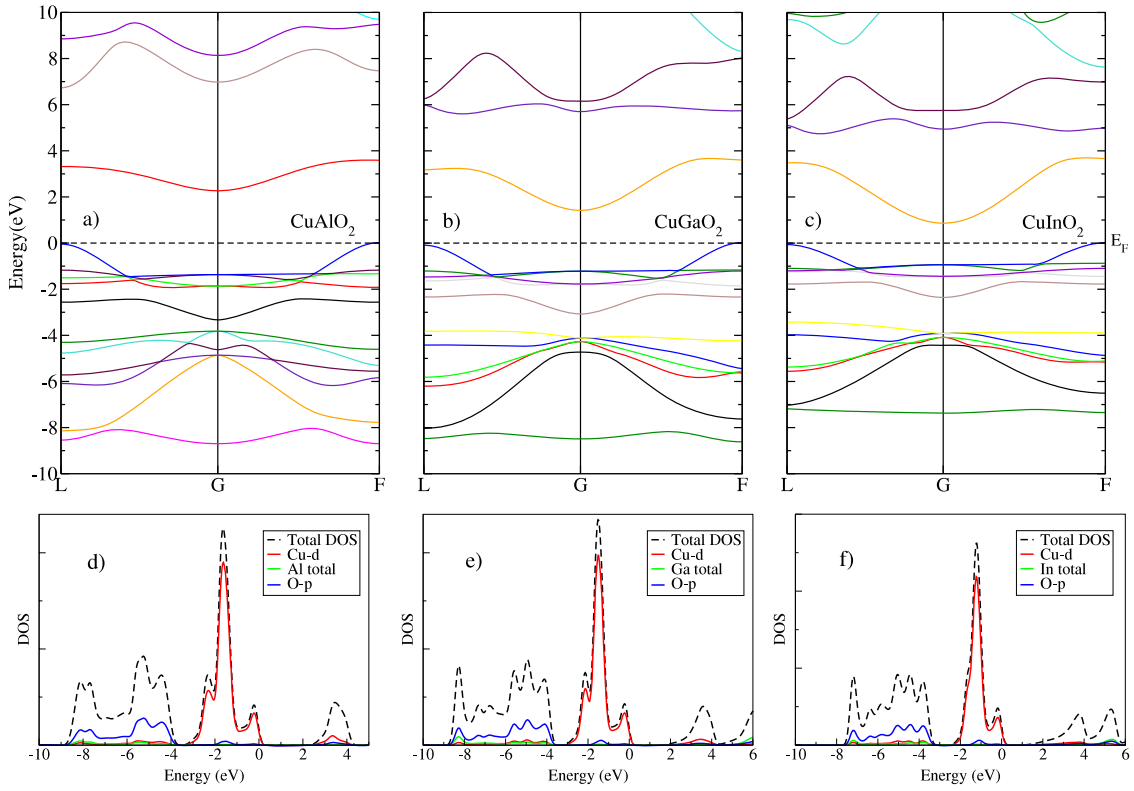

Figure 6. (a)–(c) TB-mBJ band structures and (d)–(f) DOS plots for delafossite $CuXO_2$ (X = Al, Ga, In).

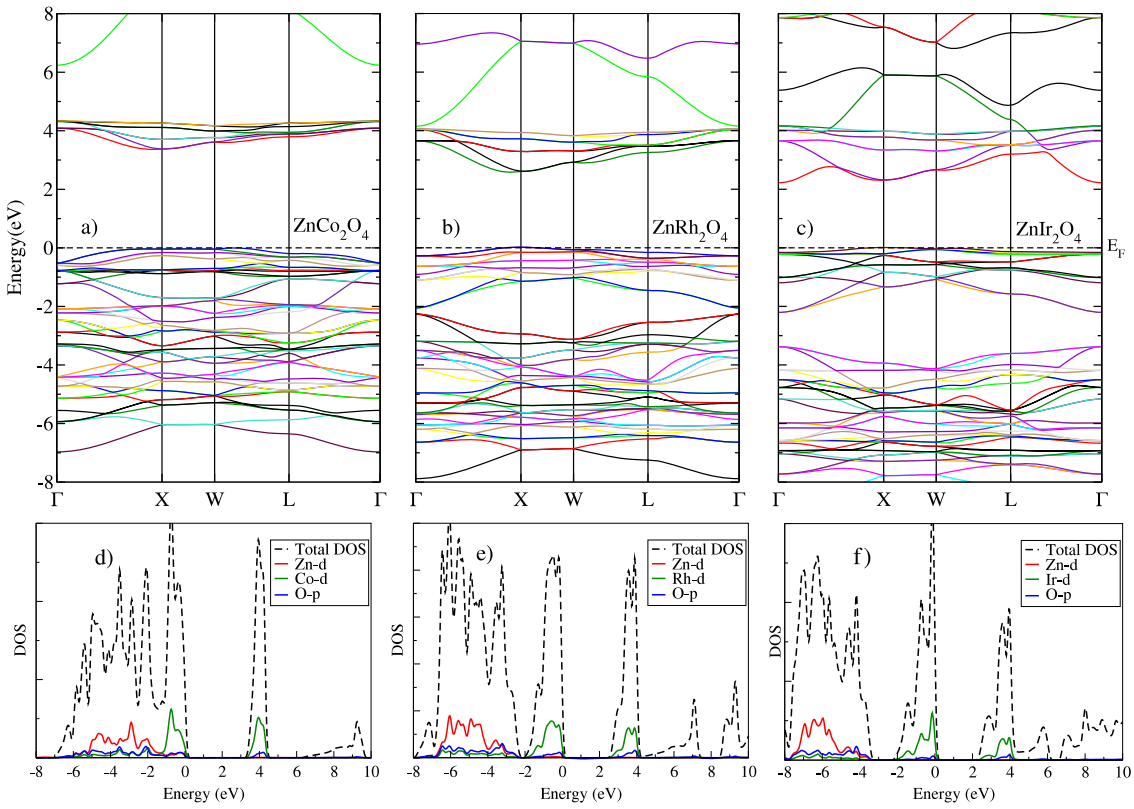

Figure 7. (a)–(c) TB-mBJ band structures and (d)–(f) DOS plots for ZnX_2O_4 (X = Co, Rh, Ir) spinel.

at L while the transition at the Γ point is optically forbidden for symmetry reasons [33, 34]. The calculated direct band gaps are 3.28, 3.14 and 3.42 eV, which are underestimated compared to the experimental values of 3.4, 3.6 and 3.9 eV by ∼3%–12% for $CuAlO_2$, $CuGaO_2$ and $CuInO_2$ respectively. The trend in the direct band gap, which slightly decreases from $CuAlO_2$ to $CuGaO_2$ and increases afterward for $CuInO_2$, is in qualitative agreement with previous PBE and G_0W_0@COHSEX results. It should be noted that the surprising overestimation of the G_0W_0 gap is attributed to polaronic effects and it has been shown that the direct gap is well reproduced by many-body approaches only if the polaronic effects are taken into account [35]. Also, $CuAlO_2$ features strong excitonic effects, with an exciton binding energy of 0.47 eV [36]. The TB-mBJ scheme cannot account for either the polaronic or the excitonic effects observed in these systems.

Other interesting systems are ZnX_2O_4 (X = Co, Rh, Ir) spinels which are reported to be p-type TCOs. The origin of the band gap in these spinels is attributed to the ligand field splitting of X d orbitals into fully occupied t_{2g}^6 and empty e_g^0 levels due to the octahedral surrounding of six oxygen anions forming a low spin state configuration. A recent theoretical study by Scanlon *et al* [37] has shown underestimation of the band gap by PBE and a severe overestimation of the t_{2g}^6–e_g^0 splitting with the HSE calculation compared to reported experimental values. Moreover, the observed decreasing trend in the band gap while moving from Co to Rh to Ir is in contrast to the only experimental study of Dekkers *et al* [9] which reports the opposite. The TB-mBJ calculated band structures and PDOSs for these spinels are shown in figure 7. All three spinels have an indirect band gap with the VBM occurring at the X point and the CBM located near the X point along the X–Γ direction. The well-isolated peaks of occupied t_{2g}^6 and empty e_g^0 levels form the VBM and CBM respectively as is evident from the PDOS. The Zn 3d states are spread in the lower part of the valence band with lowest peaks around −4.8, −6.6 and −7.2 eV which are shallow compared with the experimental report of ∼−8.8, ∼−9.2 and ∼−9.5 eV for $ZnCo_2O_4$, $ZnRh_2O_4$ and $ZnIr_2O_4$ respectively. We also observe a decreasing trend in the indirect gap while moving from Co to Rh to Ir with both PBE and TB-mBJ in accordance with the HSE result. The calculated indirect band gaps are 3.36, 2.53 and 2.30 eV for $ZnCo_2O_4$, $ZnRh_2O_4$ and $ZnIr_2O_4$ respectively (see table 5). Other experimental studies which report band gaps of 2.63 and 2.1 eV for $ZnCo_2O_4$ [8] and $ZnRh_2O_4$ [7] are at variance with Dekkers *et al* and also show a decrease in the band gap when Co is replaced by the heavier Rh cation. We find that TB-mBJ yields a better estimate of the band gap than HSE for $ZnCo_2O_4$ and $ZnRh_2O_4$ in comparison with these experiments, although the t_{2g}^6–e_g^0 splitting is overestimated. Thus the TB-mBJ calculations support the claim made by Scanlon *et al* for reinvestigation of the band gaps for these spinels.

5. Discussion and conclusions

We first discuss the results obtained for the binary oxides, namely In_2O_3, ZnO, CdO and SnO_2. The calculated band

Table 1. The PBE, TB-mBJ, G_0W_0 and experimental band gaps (all in eV) for four different oxides.

Oxide	E_g^{PBE}	E_g^{TB-mBJ}	$E_g^{Expt.}$	$E_g^{G_0W_0}$
In_2O_3	1.18	2.90	3.10[a]	3.10[b]
ZnO	0.78	2.68	3.44	2.49[c]
CdO	−0.28	1.82	1.2–2[d]	1.07[e]
SnO_2	1.25	3.20	3.60	3.85[f], 3.65[g]

[a] Reference [39].
[b] Reference [41].
[c] Reference [43].
[d] Reference [45].
[e] Reference [46].
[f] Reference [49].
[g] Reference [50].

Table 2. The electron effective masses for n-type binary oxides.

Oxide	m_e^{PBE}	m_e^{TB-mBJ}	$m_e^{Expt.}$
In_2O_3	0.22	0.54	0.30
ZnO	$m_\parallel = 0.23$	$m_\parallel = 0.51$	0.32
	$m_\perp = 0.14$	$m_\perp = 0.33$	
CdO	0.16	0.35	0.20
SnO_2	$m_\parallel = 0.17$	$m_\parallel = 0.23$	0.29
	$m_\perp = 0.29$	$m_\perp = 0.42$	

Table 3. The experimental lattice constants and the internal parameters 'u', for delafossite ([33]) and spinel ([9]) structure.

Delafossite	$CuAlO_2$	$CuGaO_2$	$CuInO_2$
a (Å)	2.858	2.963	3.292
c (Å)	16.958	17.100	17.388
u	0.1099	0.1073	0.1056
Spinel	$ZnCo_2O_4$	$ZnRh_2O_4$	$ZnIr_2O_4$
a (Å)	8.104	8.489	8.507
u	0.263	0.263	0.263

gaps along with the experimental and GW results are given in table 1. The strong underestimation of the KS gaps with PBE can partly be attributed to the overestimated p–d hybridization between the anion and cation. The p–d repulsion pushes the VBM upwards resulting in further closure of the KS gap [54]. The TB-mBJ band gaps, as listed in the second column, show a good improvement in the gaps compared to PBE. These gaps also are in agreement with the experimental values with small underestimation except for ZnO. For ZnO the band gap is underestimated by as much as 22%. It should be noted that the G_0W_0 result for ZnO is also underestimated. Since the LDA or GGA is typically used as a starting point to calculate the G_0W_0 gap, the p–d hybridization in the LDA/GGA band structure influences the result and correspondingly the G_0W_0 gap of ZnO is underestimated. For other systems which show a weaker hybridization in the LDA/GGA band structure, the agreement between the G_0W_0 and the experimental gap is remarkably well.

The TB-mBJ DOS shows that the dispersion of the upper valence band is narrowed and the lower valence bands are moved to higher binding energies by ∼0.8–1.0 eV compared

Table 4. The indirect (E_{ind}) and direct (E_{dir}) band gaps at L of the delafossite structures calculated with PBE and TB-mBJ along with reported G_0W_0 ([34]) and experimental band gaps (all in eV).

	PBE		TB-mBJ		G_0W_0		Expt.	
Oxide	E_{ind}	E_{dir}	E_{ind}	E_{dir}	E_{ind}	E_{dir}	E_{ind}	E_{dir}
$CuAlO_2$	1.92	2.57	2.21	3.28	4.96	5.05	3.00	3.4[a]
$CuGaO_2$	0.92	2.40	1.35	3.14	4.03	4.83	—	3.6[b]
$CuInO_2$	0.42	2.96	0.82	3.42	3.53	5.55	1.44	3.9[c]

[a] Reference [3].
[b] Reference [4].
[c] Reference [5].

Table 5. The indirect band gaps calculated with PBE and TB-mBJ along with reported HSE ([37]) and experimental band gaps for the spinel structure (all in eV).

Oxide	PBE	TB-mBJ	HSE	Expt.
$ZnCo_2O_4$	0.71	3.36	3.86	2.26[a], 2.63[b]
$ZnRh_2O_4$	0.89	2.53	2.87	2.74[a], 2.1[c]
$ZnIr_2O_4$	0.28	2.30	2.45	2.97[a]

[a] Reference [9].
[b] Reference [8].
[c] Reference [7].

to the PBE counterparts in the cases of ZnO and SnO_2. For In_2O_3 and CdO, this change is less significant. This might explain the better agreement between the TB-mBJ and experimental band gaps observed in the cases of In_2O_3 and CdO. Another important physical property of n-type TCO is the electron effective mass. The TB-mBJ effective masses are listed in table 2. The observed trend shows that the effective masses are systematically overestimated (almost by a factor of 2) compared to PBE values and also experiment. This agrees with similar observations recently made for III–V semiconductors by Kim *et al* [24]. This overestimation can be attributed to the general tendency of the TB-mBJ scheme to reduce the dispersion of the bands as discussed earlier.

For the p-type conducting TCOs studied, namely delafossite $CuXO_2$ (X = Al, Ga, In) and spinel ZnX_2O_4 (X = Co, Rh, Ir), we find qualitative agreement between the TB-mBJ and G_0W_0 or HSE results with respect to the trends in the band gap. Quantitatively, however, the TB-mBJ gaps are different from those reported with G_0W_0 or HSE. Moreover, we observe that the Cu d and Zn d states in these systems are also shallow compared to the experimental counterparts as was observed in the cases of ZnO and CdO. In spite of the complicated electronic structure of these systems the TB-mBJ scheme gives a better estimation of the band gap over PBE and the trends observed within G_0W_0/HSE are also reproduced. Thus we find that the TB-mBJ offers a reliable, simple way and viable alternative to the computationally expensive techniques for calculation of the band gaps of TCOs with the desired accuracy.

Acknowledgments

We gratefully acknowledge financial support from the IWT-Vlaanderen through the ISIMADE project, the FWO-

Vlaanderen through project G.0191.08 and BOF-NOI of the University of Antwerp. This work was carried out using the HPC infrastructure of the University of Antwerp (CalcUA), a division of the Flemish Supercomputer Center (VSC), which is funded by the Hercules foundation.

References

[1] Minami T 2005 *Semicond. Sci. Technol.* **20** S35
[2] Segev D and Wei S-H 2005 *Phys. Rev.* B **71** 125129
[3] Kawazoe H, Yasukawa M, Hyodo H, Kurita M, Yanagi H and Hosono H 1997 *Nature* **389** 939
[4] Yanagi H, Ueda K, Kawazoe H and Hosono H 2000 *J. Appl. Phys.* **88** 4159
[5] Ueda K, Hase T, Yanagi H, Kawazoe H, Hosono H, Ohta H, Orita M and Hirano M 2001 *J. Appl. Phys.* **89** 1790
[6] Yanagi H, Hase T, Ibuki S, Ueda K and Hosono H 2001 *Appl. Phys. Lett.* **78** 1583
[7] Mizoguchi H, Hirano M, Fujitsu S, Takeuchi T, Ueda K and Hosono H 2002 *Appl. Phys. Lett.* **80** 1207
[8] Kim H J, Song I C, Sim J H, Kim H, Kim D, Ihm Y E and Choo W K 2004 *J. Appl. Phys.* **95** 7387
[9] Dekkers M, Rijnders G and Blank D H A 2007 *Appl. Phys. Lett.* **90** 021903
[10] Mizoguchi H and Woodward P M 2004 *Chem. Mater.* **16** 5233
[11] Calnana S and Tiwari A N 2010 *Thin Solid Films* **518** 1839
[12] Hohenberg P and Kohn W 1964 *Phys. Rev.* **136** B684
[13] Kohn W and Sham L J 1965 *Phys. Rev.* **140** A1133
[14] Perdew J P, Parr R G, Levy M and Balduz J L Jr 1982 *Phys. Rev. Lett.* **49** 1691
[15] Sham L J and Schlüter M 1983 *Phys. Rev. Lett.* **51** 1888
[16] Grüning M, Marini A and Rubio A 2006 *J. Chem. Phys.* **124** 154108
[17] Grüning M, Marini A and Rubio A 2006 *Phys. Rev.* B **74** 161103(R)
[18] Heyd J, Scuseria G E and Ernzerhof M 2003 *J. Chem. Phys.* **118** 8207
[19] Heyd J, Peralta J E, Scuseria G E and Martin R L 2006 *J. Chem. Phys.* **123** 174101
[20] Aulbur W G, Jönsson L and Wilkins J W 2000 *Solid State Phys.* **54** 1
[21] Tran F and Blaha P 2009 *Phys. Rev. Lett.* **102** 226401
[22] Barcaro G, Thomas I O and Fortunelli A 2010 *J. Chem. Phys.* **132** 124703
[23] Feng W, Xiao D, Zhang Y and Yao Y 2010 *Phys. Rev.* B **82** 235121
[24] Kim Y-S, Marsman M, Kresse G, Tran F and Blaha P 2010 *Phys. Rev.* B **82** 205212
[25] Singh D J, Seo S S A and Lee H N 2010 *Phys. Rev.* B **82** 180103
[26] Singh D J 2010 *Phys. Rev.* B **82** 205102
[27] Singh D J 2010 *Phys. Rev.* B **82** 155145
[28] Gong S and Liu B-G 2011 *Phys. Lett.* A **375** 1477
[29] Johnson N W, McLeod J A and Moewes A 2011 *J. Phys.: Condens. Matter* **23** 445501
[30] Dixit H, Tandon N, Cottenier S, Saniz R, Lamoen D, Partoens B, Van Speybroeck V and Waroquier M 2011 *New J. Phys.* **13** 063002
[31] Koller D, Tran F and Blaha P 2011 *Phys. Rev.* B **83** 195134
[32] Perdew J P, Burke K and Ernzerhof M 1996 *Phys. Rev. Lett.* **77** 3865–8
[33] Nie X, Wei S-H and Zhang S B 2002 *Phys. Rev. Lett.* **88** 066405
[34] Trani F, Vidal J, Botti S and Marques M A L 2010 *Phys. Rev.* B **82** 085115
[35] Vidal J, Trani F, Bruneval F, Marques M A L and Botti S 2010 *Phys. Rev. Lett.* **104** 136401
[36] Laskowski R, Christensen N E, Blaha P and Palanivel B 2009 *Phys. Rev.* B **79** 165209
[37] Scanlon D O and Watson G W 2011 *Phys. Chem. Chem. Phys.* **13** 9667
[38] Monkhorst H D and Pack J D 1976 *Phys. Rev.* B **13** 5188
[39] Walsh A, Da Silva J L F, Wei S-H, Körber C, Klein A, Piper L F J, DeMasi A, Smith K E, Panaccione G, Torelli P, Payne D J, Bourlange A and Egdell R G 2008 *Phys. Rev. Lett.* **100** 167402
[40] Mryasov O N and Freeman A J 2001 *Phys. Rev.* **64** 233111
[41] Fuchs F and Bechstedt F 2008 *Phys. Rev.* B **77** 155107
[42] Kotani T, van Schilfgaarde M and Faleev S V 2007 *Phys. Rev.* B **76** 165106
[43] Dixit H, Saniz R, Lamoen D and Partoens B 2010 *J. Phys.: Condens. Matter* **22** 125505
[44] Singh D J 2010 *Phys. Rev.* B **82** 205102
[45] McGuinness C, Stagarescu C B, Ryan P J, Downes J E, Fu D and Smith K E 2003 *Phys. Rev.* B **68** 165104
[46] King P D C, Veal T D, Schleife A, Zúñiga-Pérez J, Martel B, Jefferson P H, Fuchs F, Muñoz-Sanjosé V, Bechstedt F and McConville C F 2009 *Phys. Rev.* B **79** 205205
[47] Fröhlich D, Kenklies R and Helbig R 1978 *Phys. Rev. Lett.* **41** 1750
[48] Batzill M and Diebold U 2005 *Prog. Surf. Sci.* **79** 47154
[49] Saniz R, Dixit H, Lamoen D and Partoens B 2010 *Appl. Phys. Lett.* **97** 261901
[50] Schleife A, Varley J B, Fuchs F, Rödl C, Bechstedt F, Rinke P, Janotti A and Van de Walle C G 2011 *Phys. Rev.* B **83** 035116
[51] Blaha P, Schwarz K, Madsen G K H, Kvasnicka D and Luitz J 2001 *WIEN2K: An Augmented Planewave + Local Orbitals Program for Calculating Crystal Properties* ed K Schwarz (Austria: Techn. Universität Wien) ISBN: 3-950131-1-2
[52] Cottenier S 2002 *Density Functional Theory and The Family of (L)APW-methods: A Step-by-step Introduction* (Belgium: Instituut voor Kern-en Stralingsfysica, KULeuven) (freely available from www.wien2k.at/reg_user/textbooks)
[53] Aston D J, Payne D J, Green A J H, Egdell R G, Law D S L, Guo J, Glans P A, Learmonth T and Smith K E 2005 *Phys. Rev.* B **72** 195115
[54] Wei S-H and Zunger A 1988 *Phys. Rev.* B **37** 8958